

## Optical, electrical and photovoltaic characteristics of organic semiconductor based on oxazine/n-Si heterojunction

A.A.M. Farag<sup>a,\*</sup>, E.A.A. El-Shazly<sup>a</sup>, M. Abdel Rafea<sup>b</sup>, A. Ibrahim<sup>c</sup>

<sup>a</sup> Thin Film Laboratory, Physics Department, Faculty of Education, Ain Shams University, Heliopolis, Roxy, Cairo, Egypt

<sup>b</sup> Institute of Advanced Technology and New Materials, Mubarak City for Scientific Research and Technology Applications, New Borg El Arab city, Alexandria, Egypt

<sup>c</sup> Solar energy Laboratory, Physics Department, Faculty of Science, Tanta University, Cairo, Egypt

### ARTICLE INFO

#### Article history:

Received 16 December 2008

Received in revised form

28 June 2009

Accepted 29 June 2009

Available online 25 July 2009

#### Keywords:

Organic–inorganic devices

Optical properties

Electrical properties

Photovoltaic characteristics

*I*–*V* and *C*–*V* characteristics

### ABSTRACT

In this work, the construction and photoelectrical characterization of p-type organic semiconductor oxazine (OXZ) in junction with n-type silicon semiconductor are presented. The Stokes shift between absorption and emission of oxazine was analyzed. The analysis of the spectral behavior of the absorption coefficient ( $\alpha$ ) of OXZ, in the absorption region revealed a direct transition, and the energy gap was estimated as 1.82 eV. From the current–voltage, *I*–*V*, measurements of the Au/OXZ/n-Si/Al heterojunction in the temperature range 300–375 K, characteristic junction parameters and dominant conduction mechanisms were obtained. This heterojunction showed a photovoltaic behavior with a maximum open circuit voltage,  $V_{oc}$ , of 0.42 V, short-circuit current density,  $J_{sc}$ , of 3.25 mA/cm<sup>2</sup>, fill factor, *FF*, of 0.35 and power conversion efficiency,  $\eta$ , of 3.2% under 15 mW/cm<sup>2</sup> white light illumination.

© 2009 Elsevier B.V. All rights reserved.

### 1. Introduction

During the last decade, focus on organic photovoltaics (OPV) devices has increased due to their low cost, low thermal budget, solution processing, flexible substrates, operational stability, very high speed of processing, environmental impact and indoor applications [1–4]. Until recently the silicon-based PVs had advantages in both efficiency and lifetime of the device for monocrystalline silicon devices. Organic solar cells have the potential to be competitive on the photovoltaic power market due to expected low production costs even with lower efficiencies and shorter lifetimes compared to their inorganic counterparts [4,5]. It should be emphasized that high efficiency and long lifetime has not been observed for the same device, and one of the current challenges is the combination of all the desirable properties in the same material (efficiency, stability, processability and low cost). The separate demonstration of these properties for different materials, however, does show that it should be possible and from this point of view, the OPVs could become a true competitor to the silicon-based PV.

Heterojunction-based semiconductor devices formed by organic compounds grown on inorganic substrates have extensively been investigated by many researchers for their potential

use in the electronic and optoelectronic technologies so far. Namely, many devices using the polymeric [6–9] and nonpolymeric organic materials [10–12] have been fabricated including light-emitting diodes and Schottky-type devices like an inorganic semiconductor/organic semiconductor material or a metal/organic semiconductor material, and their electrical and photoelectrical properties have been investigated for more than three decades. Organic materials have a wide application in thin-film electronics; one of their main advantages is the fact that they can be produced in large quantities by simple techniques such as spin coating, which lowers the production cost dramatically [13]. In recent years, power conversion efficiencies of thin-film organic photovoltaic cells have been increased steadily and rapidly [14,15]. Although higher power conversion efficiency is provided by conventional silicon-based photovoltaic devices, a large number of scientists are involved in the development of organic molecules and conjugated polymer-based photovoltaic devices [16–18].

Oxazine (OXZ) dyes have been a subject of much spectroscopic research due to their great use as a tunable laser dye in the range 600–900 nm. Alternatively, they are also the standards for fluorescence studies and are of significant value as biological probes [19]. A large number of investigations have been carried out in recent years on spectroscopic behavior of this group of dyes [20,21].

In this paper, we report the fabrication and electrical properties of rectifying heterojunction barriers using oxazine as an interlayer formed on n-Si substrate. Our aim is to study the optical

\* Corresponding author. Tel.: +202 245 580 86; fax: +202 225 812 43.  
E-mail address: [alaafaragg@yahoo.com](mailto:alaafaragg@yahoo.com) (A.A.M. Farag).

and fluorescence properties of oxazine films. We also study the suitability and possibility of organic-on-inorganic semiconductor contact barrier diodes for use in barrier modification of Si metal–semiconductor diodes using  $I$ – $V$  and  $C$ – $V$  characteristics of oxazine/n-Si heterojunction. The characteristic parameters of these devices have been obtained from their dark current–voltage and capacitance–voltage characteristics. Photovoltaic characteristics of oxazine/n-Si heterojunction under different intensities of white light illumination were also studied.

## 2. Experimental details

### 2.1. Materials

The oxazine compound, whose molecular structure is shown in Fig. 1, was purchased from AnaSpec Inc., and used without further purification as a solute. The oxazine dye appears as green bronzy crystals. The junctions have been prepared using a polished n-type Si wafer with (100) orientation and electron concentration  $10^{16} \text{ cm}^{-3}$  with thickness  $400 \mu\text{m}$  obtained from Nippon Mining company (Japan) as a substrate.

### 2.2. Solubility and stability

The oxazine dyes showed good solubility in water, ethanol and DMSO. They were found to be more photo and thermal stable than similar commercially available materials.

### 2.3. Processes and fabrication of the device

In order to remove the native oxide on surface of n-Si, the substrate was etched by a solution of  $6\text{HNO}_3:1\text{HF}:35\text{H}_2\text{O}$  for 20 s, then rinsed with deionized water and dried. The n-Si substrates were coated from one side by oxazine thin film using spin coating process. The coating solution was dropped onto substrate, which was rotated at 2000 rpm for 30 s. After the spin coating, the film was dried at 350 K for 10 min in a furnace to evaporate the solvent and to remove organic residuals. The front contact of this

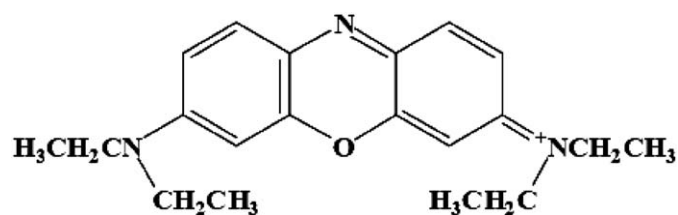


Fig. 1. Molecular structure of the OXZ organic semiconductor.

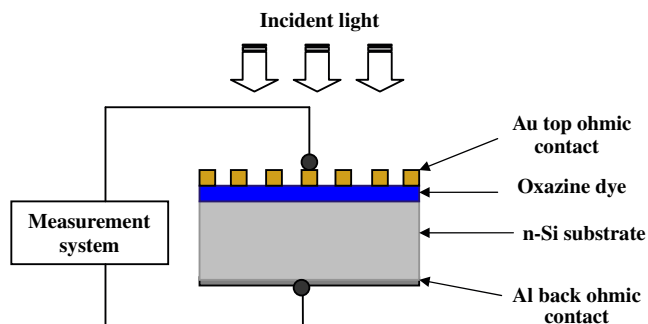


Fig. 2. Schematic diagram of Au/OXZ/n-Si/Al heterojunction.

heterojunction was made with gold mesh electrode. The active area of the fabricated heterojunction was about  $0.20 \text{ cm}^2$ . The back contact was made by depositing a relatively thick film of Al to the bottom of the n-Si substrate using thermal evaporation technique under vacuum (Edwards, E306A) at pressure about  $10^{-4} \text{ Pa}$ . Thus, an Au/OXZ/n-Si/Al junctions were obtained. The fabricated cells were annealed in air at 373 K for 1 h to complete the junction formation. The schematic diagram of the fabricated junction is shown in Fig. 2.

### 2.4. Methods and characterization tools

The absorption studies in the UV–vis spectra of the OXZ films deposited on a quartz substrate were recorded on a JASCO-570 UV/VIS/NIR spectrophotometer. Fluorescence was read on a spectrophotometer (Perkin Elmer L550B; Perkin Elmer, Wellesley, MA, USA) using excitation/emission settings of 700/900 nm.

The electrical measurements were performed using a conventional d.c. technique and a high-impedance Keithley 617 electrometer. The room temperature  $C$ – $V$  measurements of the device were achieved at 1 MHz by using computerized  $C$ – $V$  meter (model 4108, solid-state measurements, Inc. Pittsburg Pennsylvania) in air and at dark conditions. The temperature was measured directly by means of chromel–alumel thermocouple connected to a hand-held digital thermometer. The incident power density of light illumination was  $15 \text{ mW/cm}^2$  provided by a halogen tungsten lamp. Optical exposure was focused onto the Au electrodes from above the devices. The power density of illumination on the device was measured by means of a calibrated TM 20 solar power meter.

## 3. Results and discussion

### 3.1. Optical absorption characterization

The UV–vis spectrum spectra of OXZ films at room temperature (300 K) is shown in Fig. 3. It is observed that there is an absorption peak namely the Q-band in the wavelengths range 590–645 nm and a small peak at shorter wavelengths in the UV region termed Soret band (B-band) in the range 239–295 nm. The absorption peaks can be readily interpreted using the Gouterman's four-orbital model [18]. Specifically, there are two principle  $\pi$ – $\pi^*$  transitions of the oxazine ring: a lower energy

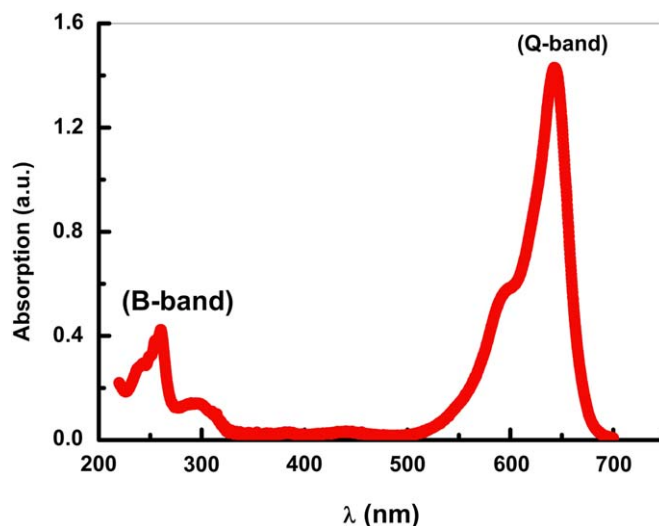


Fig. 3. The UV-vis absorption spectra of OXZ films at 300 K.

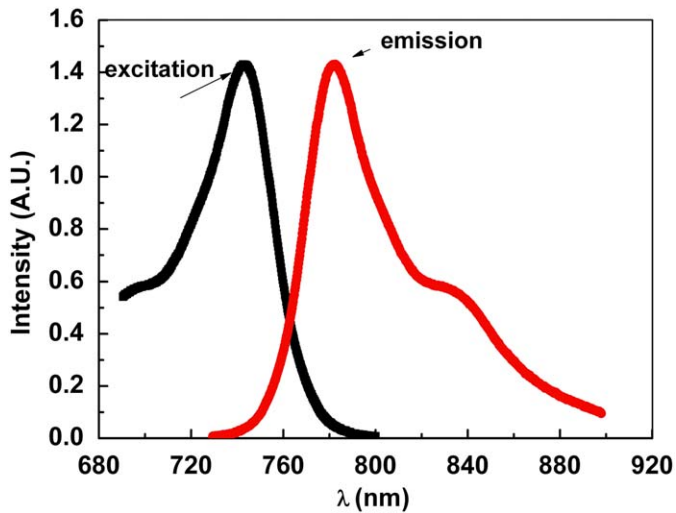


Fig. 4. Excitation-emission spectra of OXZ films at 300K.

“Q-band” is attributed to the transition from the highest occupied molecular orbital (HOMO)  $a_{1u}$  to the lowest unoccupied molecular orbital (LUMO)  $e_g$ . A higher energy “B-band” arises from the  $a_{2u}$  (HOMO)  $\rightarrow e_g$  (LUMO) transitions. The shorter wavelength band (Q) at 591 nm can be assigned to an intra molecular charge-transfer interaction. The charge transfer (CT) will originate from the sp<sup>2</sup> mixing orbital to the electron system of the macrocyclic ring of oxazine (as an origin to the C N group as a sink). The charge-transfer bands arise from the resonance of the lone pair of nitrogen atom of the aniline to the molecule substituents [19].

### 3.2. Fluorescence studies

Fig. 4 shows fluorescence emission and excitation spectra of oxazine. Fluorescence emission peaks were observed at 781 nm. The observed Stokes shift,  $\Delta = \lambda_{\text{emission}} - \lambda_{\text{excitation}}$ , was calculated as  $\sim 38$  nm. The excitation and the absorption spectra are similar and both shapes are mirror images. However, in terms of wavelength, the excitation spectrum was slightly red-shifted when compared to the absorption one.

### 3.3. Energy gap determination

To obtain information about direct or indirect inter-band transitions, the spectral dependence of the absorption coefficient  $\alpha$  near the fundamental absorption edges within the framework of band-to-band transition theory [20] was analyzed. This theory can be used to analyze the absorption edge data of many organic semiconductors [21,22]. Thus, the optical gap of the OXZ film is calculated by

$$\alpha = \left(\frac{A}{h\nu}\right)(h\nu - E_g)^m \quad (1)$$

where  $A$  is an energy independent constant,  $m$  governs the transition type and  $E_g$  the optical band gap. Differentiating the natural logarithm of Eq. (1) after multiplying by photon energy transforms the equation to be linear in  $m$  and can be also written as [23]:

$$\frac{d[\ln(\alpha h\nu)]}{d(h\nu)} = \frac{m}{h\nu - E_g} \quad (2)$$

The derivative of Eq. (1) was treated by origin lab 7 program on the calculated absorption coefficient as shown in Fig. 5. Plotting

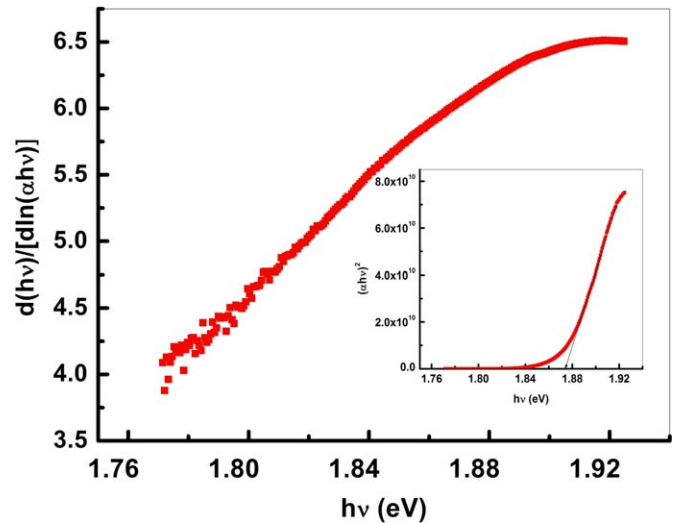


Fig. 5. Plot of  $d(h\nu)/d[\ln(\alpha h\nu)]$  vs.  $h\nu$ . The inset shows  $(\alpha h\nu)^2$  vs.  $h\nu$ .

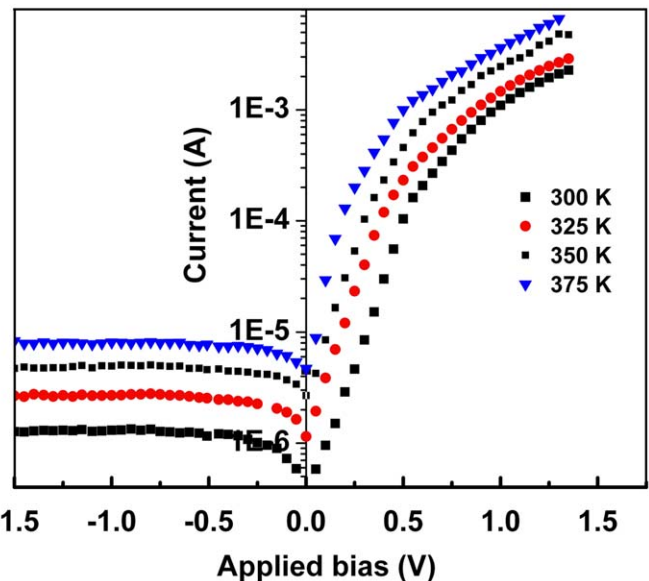


Fig. 6. The current–voltage characteristics of Au/OXZ/n-Si/Al heterojunction in the temperature range 300–375 K.

the corresponding data of the inverse on the left-hand side of Eq. (2) versus photon energy results in a linear curve in the absorption edge region only of slope  $1/m$  and intercept of  $E_g/m$ . The calculated  $m$  value is close to 0.5, which indicates that the transition type is directly allowed. The optical band gap of the film was determined from the intercept and is found to be 1.82 eV. This value of energy gap corresponds to the difference between HOMO and LUMO levels of OXZ films.

### 3.4. Electrical properties of Au/OXZ/n-Si/Al heterojunction in the dark

The analysis of the  $I$ – $V$  characteristics is extremely useful to identify the characteristic parameters as well as the transport mechanisms controlling the conduction process in the device. The current–voltage characteristics at different temperatures in the range 300–375 K is presented in Fig. 6 and it exhibits an organic/inorganic semiconductor heterojunction (OI–HJ) behavior

**Table 1**  
Parameters derived from  $I$ - $V$  characteristic for Au/OXZ/n-Si/Al heterojunction.

$T$ (K)	RR	$R_{sh}$ ( $k\Omega\text{cm}^2$ )	$R_s$ ( $\Omega\text{cm}^2$ )	$I_0$ (A)	$\Phi_b$ (eV)	$n$
300	850	35.1	27.7	$2.85 \times 10^{-7}$	0.767	3.33
325	540	21.5	21.1	$1.24 \times 10^{-6}$	0.794	3.13
350	360	11.9	11.1	$2.73 \times 10^{-6}$	0.836	2.85
375	260	7.3	7.88	$6.6 \times 10^{-6}$	0.872	2.28

with the forward direction to the negative potential on n-Si. The rectification ratio, RR, of the Au/OXZ/n-Si/Al heterojunction was calculated at 1 V at different temperatures and listed in Table 1. As observed, the structures showed that the interfacial layer formed at metal/semiconductor interface has a rectification characteristic in which the values of barrier height and ideality factor are greater than the conventional metal/semiconductor structures [24].

The remarkable interest in electrical and optical properties of organic molecular semiconductors reflects their increasingly widespread use in organic and hybrid inorganic/organic devices [25,26]. Much of this activity has been focused on the understanding and controlling key parameters such as the interface potential barriers, which can be considered later in this study. The dark  $I$ - $V$  characteristics as shown in Fig. 6 for the device consist of two distinct regions: (1) an exponential behavior at low forward bias voltages ( $V < 0.6$  V), where the current is controlled by diode characteristics. (2) a linear region at higher voltages ( $0.6 \leq V \leq 1.5$  V), where the current is limited by another conduction mechanism. The exponential behavior of  $I$ - $V$  characteristics depends on the property of the depletion region in the OXZ/n-Si interface. The  $I$ - $V$  characteristics in the exponential region depend on two parameters, i.e. ideality factor ( $n$ ) and reverse saturation current ( $I_0$ ). The ideality factor gives information about the recombination process, which takes place in the device and shape of the interfaces, i.e. the internal bulk morphology for organic devices. The second parameter that affects the exponential part of the  $I$ - $V$  characteristics is the saturation current, which gives the number of charges able to overcome the barrier under reverse bias. The present device shows exponential behavior in the voltage range  $V < 0.6$  V. This exponential dependence at this voltage range can be attributed to the formation of depletion region between OXZ and Si due to the high work function of the two ohmic contacts for OXZ and n-Si. The  $I$ - $V$  characteristics presented in Fig. 6 can be described as follows [27]:

$$I = I_{01} \left[ \exp\left(\frac{qV}{n_1 kT}\right) - 1 \right] + I_{02} \left[ \exp\left(\frac{qV}{n_2 kT}\right) - 1 \right] + \frac{q(V - IR_s)}{R_{sh}} \quad (3)$$

where  $I_0$  is the reverse saturation current,  $q$  the electronic charge,  $V$  the applied voltage,  $k$  the Boltzmann's constant,  $T$  the temperature and  $n$  is the ideality factor,  $R_s$  and  $R_{sh}$  are series and shunt resistances, respectively. The subscripts 1 and 2 indicated that two possible contributions to the diode current can be presented. The series ( $R_s$ ) and shunt resistances ( $R_{sh}$ ) are determined from the plot of diode resistance ( $R_j$ ), against voltage ( $V$ ), where  $R_j = \partial V / \partial I$ , which have been determined from the  $I$ - $V$  characteristics. A plot of  $R_j$  against voltage ( $V$ ) at different temperatures is shown in Fig. 7. It was observed that at sufficient high forward voltage, the junction resistance approaches to a constant value, which is the series resistance ( $R_s$ ) (the sum of total resistance values of the resistors in series and resistance in semiconductor device in the direction of current flow). On the other hand, the junction resistance is also constant at high reverse bias, which is equal to the diode shunt resistance ( $R_{sh}$ ) (a high-precision resistor, which can be used to measure the

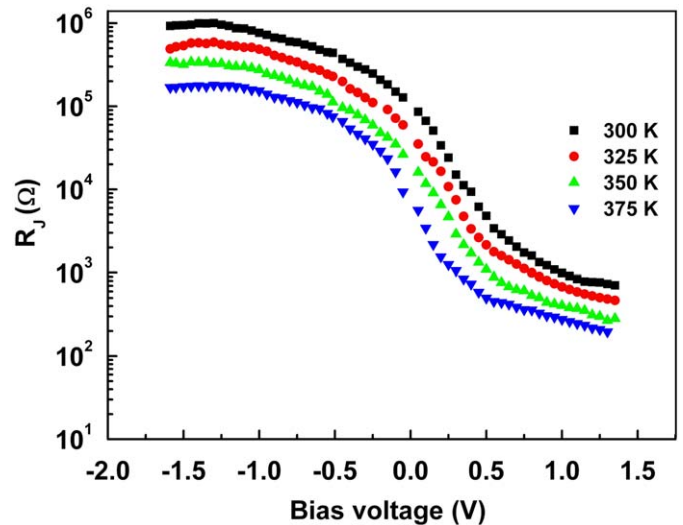


**Fig. 7.** Junction resistance under bias voltage of Au/OXZ/n-Si/Al heterojunction in the temperature range 300–375 K.

leakage current flowing through a device). The values obtained for the series and shunt resistances at different temperatures are given in Table 1. Increase in  $R_s$  with fall in temperature is believed to be a result of the lack of free carrier concentration at low temperatures [28]. The information about the conduction mechanism can be obtained from the  $I$ - $V$  characteristics at different temperatures. In a narrow voltage range ( $V < 0.6$  V), the forward current increases exponentially. A similar behavior was obtained by other authors [29,30] for organic/inorganic heterojunction devices. They showed a large number of Schottky barriers have been prepared and characterized using organic conductive polymers with metals and inorganic semiconductors. This opens a new possibility of replacing conventional inorganic devices by organic ones [36]. The junction current-voltage relationship obeys the thermionic emission as follows [24]:

$$I = I_0 \left[ \exp\left(\frac{qV}{nkT}\right) - 1 \right] \quad (4)$$

The reverse saturation current  $I_0$  is given by

$$I_0 = AA^* T^2 \exp\left(-\frac{q\Phi_B}{kT}\right) \quad (5)$$

where  $A$  is the effective area of the diode,  $A^*$  the effective Richardson constant usually taken as  $120 \text{ A/cm}^2 \text{ K}^{-2}$  for free electrons [24] and  $\Phi_B$  the barrier height of the diode. The  $I_0$  values at different temperatures are calculated extrapolating the linear voltage region ( $V < 0.6$  volt) of the curve to zero applied bias voltage and given in Table 1. The values of  $I_0$  at different temperatures are quite low due to the organic layer. This suggests that the organic OXZ layer modifies the electrical properties of the n-Si diode. When Au/OXZ/n-Si/Al heterojunction diode with  $R_s$  is considered, it assumed that the net current of the diode is due to thermionic emission theory and it can be expressed as for  $V \geq 3kT/q$

$$I = I_0 \left[ \exp\left(\frac{q(V - IR_s)}{nkT}\right) - 1 \right] \quad (6)$$

Here the term of  $(V - IR_s)$  is equal to the voltage drop across the diode (VD).

The ideality factor  $n$  for Au/OXZ/Si/Al heterojunction diode is calculated from the slope of the  $I$ - $V$  curve (Eq. (8)):

$$n = \frac{q}{kT} \left( \frac{d(V - IR_s)}{d \ln I} \right) \quad (7)$$

The ideality factor and the barrier height are determined from forward  $I$ - $V$  characteristic at different temperatures and are listed in Table 1. It was observed that the ideality factor decreases from 3.33 to 2.28 as the temperature increases from 300 to 375 K. Deviation of  $n$  far from unity may be attributed to either recombination of electrons with holes in the depletion region, and/or the increase in the diffusion current due to increase in the applied voltage [24]. The higher values of the ideality factor,  $n > 2$ , in our prepared junctions may be attributed to factors such as interfacial layer thickness, leakage, shunting, bulk series resistance, or any resistive loss [24–29]. The calculated barrier height of the studied diode is lower than that of Ni/n-Si diode (0.9 eV) [28]. This suggests that the OXZ organic layer modifies the barrier height value. The organic layer can produce substantial shift in the work function of the metal and in the electron affinity of the semiconductor by giving an excess for the barrier height, i.e., the barrier height of Au/n-Si diode decreases by the insertion of organic layer between n-Si semiconductor and metal. The studies in the literature have shown that effective Schottky barrier could be either increased or decreased by using organic thin layer on inorganic semiconductor [26]. It is evaluated that the interface properties of the diode is passivated by using organic layer surface to reduce the interaction between metal and Si. Furthermore, the realignments between the lowest unoccupied molecular orbital, the highest occupied molecular orbital of the organic semiconductor and the work function of the metal, in the electron affinity of the semiconductor at the organic/inorganic semiconductor interface can cause a decrease in barrier height. Indeed, modification of semiconductor surfaces by molecules can lead to the changes in the electronic properties of the metal–semiconductor devices. The presence of an oxide film plus the organic OXZ layer at Au/n-Si interface causes the non-ideal  $I$ - $V$  behavior. In order to understand which mechanisms control the device behaviors in the high-voltage region  $0.6 \leq V \leq 1.5$  V, the  $I$ - $V$  characteristics of Au/OXZ/n-Si/Al heterostructures are presented in log–log scale (at different temperatures) in Fig. 8. The dependencies become close to  $IV_m$ , where  $m > 2$ , for Au/OXZ/n-Si/Al heterostructures. The observed transition to super-linear

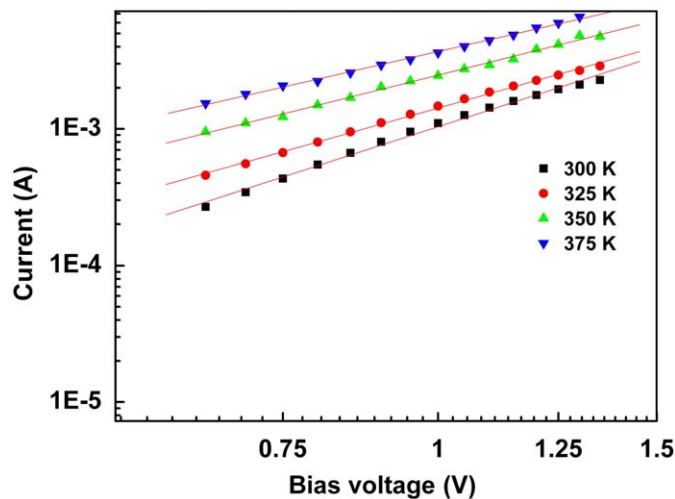


Fig. 8. Junction current under high bias voltage region of Au/OXZ/n-Si/Al heterojunction in the temperature range 300–375 K.

dependence of the current with increase in the bias voltage usually indicates the onset of a space charge limited current (SCLC) regime. The value of exponent  $m$  decreases with increasing temperature [31]. This suggests that the total trap density decreases with temperature increase. Such power dependence indicates a space charge limited conductivity (SCLC), which is characterized by an exponential distribution of trapping levels in the band gap of the organic layer (OXZ). The SCLC conduction becomes important when the density of injected free-charge carriers is much larger than the thermally-generated free charged carrier density. Thus, the SCLC current density dominated by exponential distribution of traps in the band gap of the organic thin film is given by [32]

$$I = Ae\mu N_v \left( \frac{\varepsilon_0 \varepsilon_r}{e P_0 k T_c} \right)^l \frac{V^{l+1}}{d^{2l+1}} \quad (8)$$

where  $\varepsilon$  is the dielectric constant of the organic semiconductor,  $\varepsilon_0$  the permittivity,  $\mu$  the charged carrier mobility,  $N_v$  the effective density of states in valence band edge,  $d$  the thickness of the sample and  $T_c$  the temperature parameter, which characterizes the trap distribution and describes how fast the defects fall off with the energy and  $l = T_c/T$ , where  $T$  is the ambient temperature and  $P_0$  the concentration per unit energy range at the valence band edge. The exponential trap distribution may be described in terms of  $T_c$  as [32]

$$P_{(E)} = P_0 \exp\left(-\frac{E}{kT_c}\right) \quad (9)$$

where  $P_{(E)}$  is the trap concentration per unit energy range at an energy  $E$  above the valence band. The total concentration of traps is given by

$$N_t = P_0 k T_c \quad (10)$$

From the slope ( $l+1$ ) of  $\log(I)$  vs  $\log(V)$  plot, we deduced the temperature parameter  $T_c$  value as 895 at 300 K for Au/OXZ/n-Si/Al heterostructures. A full analysis method of these results described elsewhere [32] by adopting the values of  $N_t = 2.9 \times 10^{21} \text{ m}^{-3}$  derived from the slope of the temperature dependence of the current in the SCLC region (Fig. 9). This yields a value of  $P_0 = 2.3 \times 10^{41} \text{ J}^{-1} \text{ m}^{-3}$  using Eq. (10), which together with the value of  $T_c$  fully characterizes the trap distribution of Eq. (9).

Capacitance was measured in dark as a function of reverse applied bias ( $V$ ) at 1 MHz for Au/OXZ/n-Si/Al structure in order to identify the type of the interfacial barrier. Differential capacitance measurements on a barrier measure the response of the barrier to

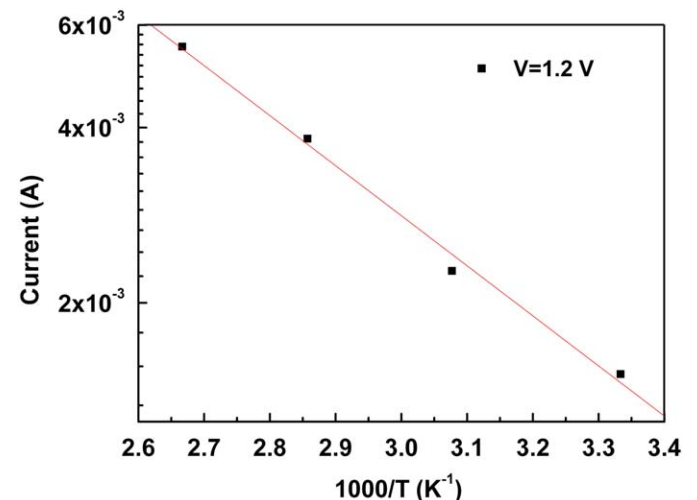


Fig. 9. Temperature dependence of the current in the SCLC region.

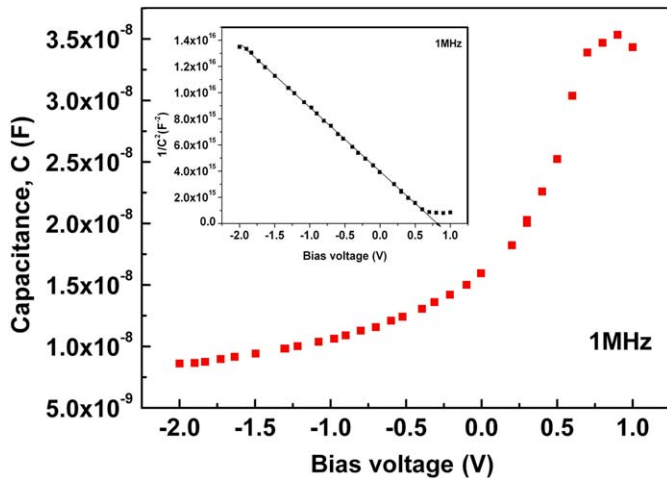


Fig. 10. High-frequency capacitance–voltage characteristics at room temperature, the inset is the  $1/C^2$  vs. bias voltage.

an alternating voltage (ac) superposed on a direct current (dc) voltage. When the dc voltage corresponds to a reverse bias, the differential capacitance represents the response of the depletion layer to the ac signal. Fig. 10 shows the forward and reverse bias  $C$ – $V$  characteristics of the structure at room temperature.

Measurement of the depletion region capacitance under forward bias is difficult because the diode is conducting and the capacitance is shunted by a large conductance. However, the capacitance can be easily measured as a function of the reverse bias. The inset of Fig. 10 shows detailed reverse  $C^2$ – $V$  plots of the Au/OXZ/n-Si/Al junction at 1 MHz. As discussed in [31], free carrier concentration and barrier height have been calculated as  $1.7 \times 10^{15} \text{ cm}^{-3}$  and 1.52 eV, respectively, from linear region of its  $C^2$ – $V$  characteristics. As seen from the values, the difference between  $\Phi_b(I-V)$  and  $\Phi_b(C-V)$  for the Au/OXZ/n-Si/Al device originates from the different nature of the  $I$ – $V$  and  $C$ – $V$  measurements. Due to different nature of the  $C$ – $V$  and  $I$ – $V$  measurement techniques, barrier heights deduced from them do not always have the same value. The capacitance  $C$  is insensitive to potential fluctuations on a length scale of less than the space charge region and  $C$ – $V$  method averages over the whole area and measures to describe the  $\Phi_b$ . The dc current across the interface depends exponentially on barrier height and thus sensitively on the detailed distribution at the interface [24]. Additionally, the discrepancy between the barrier height values of the devices may also be explained by the existence of an interfacial native oxide layer and trap states at Au/OXZ/n-Si/Al interface [31]. The junction capacitance has been measured as a function of frequency and voltage (Fig. 12).

### 3.5. Photovoltaic properties of the Au/OXZ/n-Si/Al structure

The illuminated  $I$ – $V$  characteristics of the Au/OXZ/n-Si/Al heterojunction are shown in Figs. 11 and 12. The current value at a given voltage for this device under illumination is higher than in the dark. This indicates that the absorption of light by the active layer generates carriers contributing photocurrent due to the production of excitons and their subsequent dissociation into the free-charge carriers at the barrier, i.e. OXZ–Si interface. It is observed that the photocurrent in the device in reverse direction is strongly enhanced by photoillumination. This behavior yields useful information on the electron–hole pairs, which were effectively generated in the junction by incident photons. Under the influence of the electric field at the junction, the free electrons

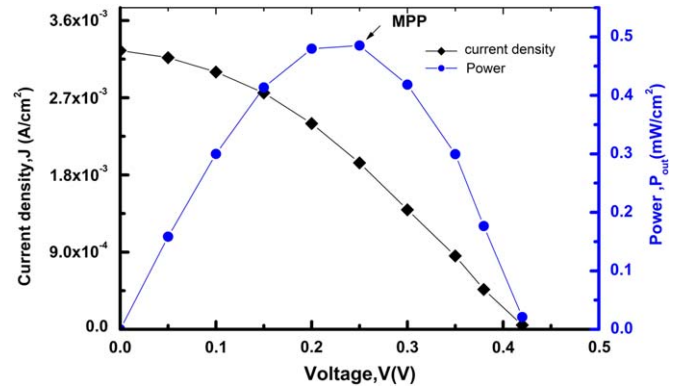


Fig. 11. Current density–voltage and power–voltage characteristics.

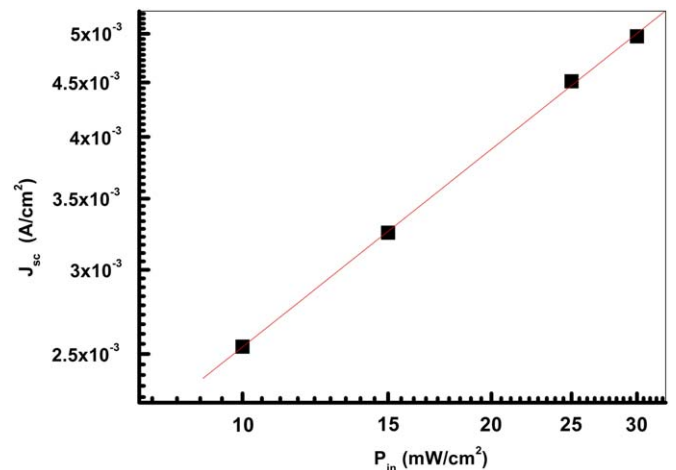


Fig. 12. Short-circuit current–power characteristics.

and holes were accelerated towards the electrodes along the potential barrier at the interface. As observed from Fig. 11, the device shows photovoltaic characteristics with short-circuit photocurrent density ( $J_{sc}$ ) (The current flowing freely through an external circuit that has no load resistance; the maximum current possible.) of  $3.25 \times 10^{-3} \text{ A/cm}^2$ , open circuit voltage ( $V_{oc}$ ) (the difference of electrical potential between two terminals of a device when there is no external load connected) of 0.42 V, fill factor ( $FF$ ) (The ratio of a solar (photovoltaic) cell's actual power to its power if both current and voltage were at their maxima.) of 0.355 and power conversion efficiency ( $\eta$ ) (The amount of energy produced as a percentage of the amount of energy consumed. In the case of a photovoltaic device, the ratio of the electric energy produced by the device, under one-sun conditions, to the energy from sunlight incident upon the cell.) of 3.2%. This value of  $\eta$  is less in comparison to those of solar cells based on conjugated polymers. The main cause of this effect is generally found to be the field-dependent nature of the charge photo generation process or high series resistance of OXZ layer. The variation of short-circuit photocurrent ( $J_{sc}$ ) with the incident light intensity ( $P_{in}$ ) for OXZ/n-Si device is shown in Fig. 12. The  $J_{sc}$  follows the power law, i.e.  $J_{sc} \propto (P_{in})^s$ , with exponent ( $s$ ) is 0.62. The  $s$  values for 0.5 and 1.0 correspond to bimolecular recombination and monomolecular recombination mechanism, respectively [33]. The value of the exponent lies between 0.5 and 1.0 for continuous distribution of trapping centers [33]. The obtained  $s$  value for the Au/OXZ/n-Si/Al diode indicates the presence of continuous distribution of traps. This value suggests that lifetime of the photocarriers are controlled by trap centers.

#### 4. Conclusion

It has been demonstrated that the Au/OXZ/n-Si/Al structure fabricated by spin coating of OXZ on n-Si substrate showed a good rectifying behavior. The current–voltage characteristics at low forward bias showed that the thermionic is the dominant charge transport mechanism through the device as well as space charge limited conduction at high forward bias. The values of the Ideality factor and barrier height have been calculated at different temperatures. The discrepancy between barrier height obtained from  $I$ – $V$  and  $C$ – $V$  measurements has been explained by introducing a spatial distribution of barrier especially due to the presence of an interface layer and barrier height inhomogeneities that prevail at the OXZ/n-Si interface. Various photovoltaic parameters were obtained from the analysis of loaded  $I$ – $V$  characteristics under illumination. The low value of the fill factor and power conversion efficiency can be attributed to the high recombination rate of carrier and consequently limited the collection efficiency of the charge carriers.

#### References

- [1] M. Niggemann, B. Zimmermann, J. Haschke, M. Glatthaar, A. Gombé, Organic solar cell modules for specific applications—from energy autonomous systems to large area photovoltaics, *Thin Solid Films* 516 (2008) 7181–7187.
- [2] F.C. Krebs, H. Spanggaard, T. Kjær, M. Biancardo, J. Alstrup, Large area plastic solar cell modules, *Mater. Sci. Eng. B* 138 (2007) 106–111.
- [3] E. Bundgaard, F.C. Krebs, Low band gap polymers for organic photovoltaics, *Sol. Energy Mater. Sol. Cells* 91 (2007) 954–985.
- [4] C. Lungenschmied, G. Dennler, H. Neugebauer, S.N. Sariciftci, M. Glatthaar, T. Meyer, A. Meyer, Flexible, long-lived, large-area, organic solar cells, *Sol. Energy Mater. Sol. Cells* 91 (2007) 379–384.
- [5] F.C. Krebs, Air stable polymer photovoltaics based on a process free from vacuum steps and fullerenes, *Sol. Energy Mater. Sol. Cells* 92 (2008) 715–726.
- [6] F.C. Krebs, Fabrication and processing of polymer solar cells: a review of printing and coating techniques, *Sol. Energy Mater. Sol. Cells* 93 (2009) 394–412.
- [7] M. Jorgensen, K. Norrman, F.C. Krebs, Stability/degradation of polymer solar cells, *Sol. Energy Mater. Sol. Cells* 92 (2008) 686–714.
- [8] T. Kıcoglu, M.E. Aydın, Y.S. Ocak, The determination of the interface state density distribution of the Al/methyl red/p-Si Schottky barrier diode by using a capacitance method, *Physica. B* 388 (1,2) (2006) 244–248.
- [9] F. Yakuphanoglu, The current–voltage characteristics an inhomogeneous-barrier analysis of ddq/p-type Si/Al diode with interfacial layer, *Physica. B* 389 (2007) 306–310.
- [10] J. Brabec, Organic photovoltaics: technology and market, *Sol. Energy Mater. Sol. Cells* 83 (2004) 273–292.
- [11] G. Syrokostas, M. Giannouli, P. Yianoulis, Effects of paste storage on the properties of nanostructured thin films for the development of dye-sensitized solar cells, *Renewable Energy* 34 (2009) 1759–1764.
- [12] F. Zhang, Y. Luo, J. Song, X. Guo, W. Liu, C. Ma, Y. Huang, M. Ge, Z. Bo, Q. Meng, Triphenylamine-based dyes for dye-sensitized solar cells, *Dyes Pigm.* 81 (2009) 224–230.
- [13] C. Siegers, B. Olah, U. Würfel, J. Hohl-Ebinger, A. Hinsch, R. Haag, Donor–acceptor-functionalized polymers for efficient light harvesting in the dye solar cell, *Sol. Energy Mater. Sol. Cells* 93 (2009) 552–563.
- [14] Y. Zhao, Z. Xie, C. Qin, Y. Qu, Y. Geng, L. Wang, Enhanced charge collection in polymer photovoltaic cells by using an ethanol-soluble conjugated polyfluorene as cathode buffer layer, *Sol. Energy Mater. Sol. Cells* 93 (2009) 604–608.
- [15] N. Ghoneim, Interface state mapping in a Schottky barrier of the organic semiconductor terrylene, *Spectrochim. Acta Pt. A* 56 (2000) 1003–1010.
- [16] A. Ghanadzadeh, A. Zeini, A. Kashef, M. Moghadam, Concentration effect on the absorption spectra of oxazine1 and methylene blue in aqueous and alcoholic solutions, *J. Mol. Liq.* 138 (2008) 100–106.
- [17] A. Jafari, A. Ghanadzadeh, H. Tajalli, M. Yeganeh, M. Moghadam, Electronic absorption spectra of cresyl violet acetate in anisotropic and isotropic solvents, *Spectrochim. Acta Pt. A* 66 (2007) 717–725.
- [18] M. Gouterman, *The Porphyrins. Part A. Physical Chemistry*, vol. III, Academic Press, New York, NY, 1978.
- [19] M.M. El-Nahass, H.M. Zeyada, K.F. Abd-El-Rahman, A.A.M. Farag, A.A.A. Darwish, Fourier-transform infrared and optical absorption spectra of 4-tricyanovinyl-N, N-diethylaniline thin films, *Spectrochim. Acta Pt. A* 69 (2008) 205–210.
- [20] G.A. Kumar, J. Thomas, N. George, B.A. Kumar, P. Radhakri, V.P.N. Shnan, C.P.G. Poori, N.V. Vallabhan, Unnikrishnan, Optical absorption studies of free (Hsp<sub>2</sub>Pc) and rare earth (RePc) phthalocyanine doped borate glasses, *Phys. Chem. Glasses* 41 (2000) 89–93.
- [21] M.M. El-Nahass, K.F. Abd-El-Rahman, A.A.M. Farag, A.A.A. Darwish, Optical characterisation of thermally evaporated phthalocyanine thin films, *Int. J. Modern Phys. B* 18 (2004) 421–434.
- [22] M.M. El-Nahass, H.S. Soliman, H.S. Metwally, A.M. Farid, A.A.M. Farag, A.A. El-Shazly, Optical properties of evaporated Iron Phthalocyanine (FePc) thin films, *J. Opt.* 30 (2001) 121–129.
- [23] M.W. Charles, H. Nick Jr., E.S. Gregory, *Physical Properties of Semiconductors*, Prentice-Hall, Englewood Cliffs, NJ, 1989.
- [24] E.H. Rhoderick R.H. Williams, *Metal–Semiconductor Contacts*, Clarendon, Oxford, (1998) 77–126.
- [25] T. Kampen, A. Schuller, D.R.T. Zahn, B. Biel, J. Ortega, R. Perez, F. Flores, Schottky contacts on passivated GaAs(100) surfaces: barrier height and reactivity, *Appl. Surf. Sci.* 234 (1–4) (2004) 341–348.
- [26] M.M. El-Nahass, K.F. Abd-El-Rahman, A.A.M. Farag, A.A.A. Darwish, Photovoltaic properties of NiPc/p-Si (organic/inorganic) heterojunctions, *Org. Electron.* 6 (2005) 129–136.
- [27] J.C. Renuarez, R.J. Garice-Sanchez, A. Ortiz-Conde, Procedure for determining diode parameters at very low forward voltage, *Solid State Electron.* 43 (1999) 2129–2133.
- [28] M. Cakar, Y. Onganer, A. Turut, The nonpolymeric organic compound (pyronine-B)/p-type silicon/Sn contact barrier devices, *Synth. Met.* 126 (2002) 213–218.
- [29] R.K. Gupta, R.A. Singh, Preparation and characterization of polymer composites of polyaniline with poly (vinyl chloride) and polystyrene, *J. Non-Cryst. Sol.* 351 (2005) 2022–2028.
- [30] M.E. Aydın, F. Yakuphanoglu, Jae-Hoon Eom, D. Hwang, Electrical characterization of Al/MEH-PPV/p-Si Schottky diode by current–voltage and capacitance–voltage methods, *Physica B* 387 (1–2) (2007) 239–244.
- [31] K. Ocakoglu, F. Yakuphanoglu, J.R. Durrant, S. Icli, The effect of temperature on the charge transport and transient absorption properties of K27 sensitized DSSC, *Sol. Energy Mater. Sol. Cells* 92 (2008) 1047–1053.
- [32] T.S. Shafai, T.D. Anthopoulos, Junction properties of nickel phthalocyanine thin film devices utilisingindium injecting electrodes, *Thin Solid Films* 398–399 (2001) 361–367.
- [33] F. Yakuphanoglu, Photovoltaic properties of the organic–inorganic photo-diode based on polymer and fullerene blend for optical sensors, *Sens. Actuators A* 141 (2008) 383–389.